Mon. Not. R. astr. Soc. (1991) **252,** 414–427

EXOSAT observations of clusters of galaxies – I. The X-ray data

A. C. Edge* and G. C. Stewart
X-ray Astronomy Group, Leicester University, Leicester LE1 7RH

Accepted 1991 May 30. Received 1991 May 30; in original form 1990 December 17

SUMMARY

X-ray observations of 45 clusters of galaxies made with the European X-ray Observatory Satellite, *EXOSAT*, are presented. The 0.1–20 keV spectra obtained constitute the largest homogeneous spectral sample presently available. Here the analysis of the spectral and imaging data is described. A significant scatter in the correlation between the X-ray luminosity and temperature, which can be interpreted as variations in the ratio of the gas mass to total mass amongst the clusters, is found. The measured iron abundances are consistent with a 'canonical' average value of 0.3 solar. The large majority of clusters are found to be cooling in their cores, indicating that cooling flows are a common phenomenon.

1 INTRODUCTION

Clusters of galaxies are prodigious X-ray emitters and a number of X-ray astronomy satellites have produced samples of detected clusters (*UHURU*, Jones & Forman 1978; *OSO-8*, Mushotzky *et al.* 1978 and Smith, Mushotzky & Serlemitsos 1979; *Ariel-V*, Mitchell *et al.* 1979; *HEAO-1*, Mushotzky 1984, Kowalski *et al.* 1984; the *Einstein Observatory*, Jones & Forman 1984, Stewart *et al.* 1984). These samples have shown strong correlations with the X-ray properties and with the optical properties. These correlations provide strong constraints on models for the current state and evolution of clusters (Cavaliere & Fusco-Femiano 1976; de Young 1978). The X-ray properties of clusters are comprehensively reviewed by Sarazin (1988).

This paper presents an analysis of the data for all the clusters observed by *EXOSAT*. Many of the observations used in this work formed part of a systematic programme to observe the brighter clusters. Others were retrieved from the *EXOSAT* database. This sample represents the largest, homogeneous, high-quality spectral dataset presently available. Here the spectral and imaging results are presented and the relationships between the X-ray properties of clusters are investigated. In a following paper, comparisons with other cluster properties are made and their implications discussed (Edge & Stewart 1991, Paper II).

2 DATA

A full review of the *EXOSAT* mission can be found in White & Peacock (1988). Briefly, the *EXOSAT* observatory carried two low-energy telescopes, LE (de Korte *et al.*, 1981), a medium-energy array of proportional counters, ME (Turner, Smith & Zimmerman 1981) and a gas scintillation counter, GSPC (Peacock *et al.* 1981). The LE was sensitive between 0.1 and 2.0 keV but provided no spectral resolution. However, with the use of filters, the LE provided some 'multicolour' photometric information. The ME was sensitive between 1.5 and 20 keV and had an energy resolution of 20 per cent at 6.7 keV. The GSPC had a passband between 3 and 40 keV and had an energy resolution of 12 per cent at 6.7 keV, but its lower sensitivity meant that it did not offer any improvement over the more sensitive ME for any cluster. We have therefore used only the ME and LE data in the spectral analysis.

EXOSAT observed three nearby clusters (Virgo, Coma and Perseus) extensively in a series of offset observations to obtain limited spatial resolution with the 45×45 arcmin^2 field of view of the ME. The observations of these three clusters are presented in Edge & Stewart (1988), Hughes, Gorenstein & Fabricant (1988) and Edge (1989) respectively.

3 ANALYSIS

3.1 LE images

Source positions, count rates and surface brightness profiles were determined from images created with the LE data. The thin Lexan filter had the highest transmission and was therefore used in all observations. Nine observations also had Aluminium/Parylene filter exposures and two had Boron filter exposures. These observations gave detections but with notably lower signal-to-noise ratios. The surface brightness profiles were integrated out to 10–20 arcmin (depending on the redshift and position in the detector) to give approximate count rates for the whole cluster. These count rates were used with the ME data to derive spectral fits over the full 0.1–20 keV band.

The surface brightness profiles were analysed using the deprojection method described in Fabian *et al.* (1981), Stewart *et al.* (1984) and Arnaud (1988). These deprojec-

*Present Address: Institute of Astronomy, Madingley Road, Cambridge CB3 0HA.

tions give estimates for the temperature and density profiles and, where the central cooling time is less than the Hubble time, the mass flow rate. A Monte-Carlo technique was used to estimate the errors on the physical parameters following the approach of Arnaud (1988) of perturbing the original count profile by Poisson errors and repeating the deprojection on 200 perturbed profiles. Published core radii from the *Einstein Observatory* have also been used in the analysis for this paper.

3.2 ME spectra

Spectra were obtained from the ME data by subtracting background from the pointed data either from slew observations before or after the pointing, or from the offset halves (where the pointing contained an array swap). For the clusters with more than one pointing, the data from the central pointing are used. Fig. 1 presents spectral fits for two clusters showing the range in the signal-to-noise ratios for the sample.

These spectra were then fitted, in conjunction with the corrected LE count rates, with optically-thin metal-enriched plasma bremsstrahlung spectra calculated using the Raymond & Smith (1977) code. All elemental abundances relative to hydrogen were fixed at half the solar value (consistent with measurements for a small number of clusters with the *Einstein* Observatory SSS detector) except for helium, fixed at the solar value, and iron ($Fe/H = 4 \times 10^{-5}$) which was a free parameter in the fit as the 6.7-keV blend of iron was significantly detected in the ME spectra. The spectral fitting gave temperatures, iron abundances, column densities and fluxes for each spectrum.

4 NOTES ON THE SAMPLE

The original goal of this spectral survey was to observe all 31 clusters in the high galactic latitude sample from *HEAO-1* (Piccinotti *et al.* 1982). Unfortunately *EXOSAT* only observed 18 of these clusters in the three years of operation, so the sample is not 'complete' in itself. However, when combined with *Einstein observatory* data, a 'complete' sample can be obtained (Edge *et al.* 1990). In addition to the 18 Piccinotti clusters, a further 22 clusters at low galactic latitude or with fluxes below the Piccinotti flux limit were observed. Thirty-four clusters in the sample were also observed by the *Einstein Observatory*. Table 1 lists the *EXOSAT* observations and gives an LE count rate for each detection. *EXOSAT* observations of seven clusters have been published by other authors. These previous analyses are listed in Table 2. Only one previously published *EXOSAT* cluster (2008 − 56) is not presented here (Piro & Fusco-Femiano 1988). The data from this cluster were obtained from one offset quadrant of an observation of another target (RR Tel). The flux for the cluster is poorly determined due to the uncertainties in the cluster position in the ME field of view. For this reason this cluster was not included in this analysis although the temperature quoted by Piro & Fusco-Femiano (1988) of 5.3 keV is consistent with the other clusters in this sample.

There are a number of clusters which merit individual mention:

(i) Triangulum Australis – this cluster was noted in the *Ariel-V* and *HEAO-1 A-1* surveys (McHardy *et al.* 1981; Remillard, private communication). It is bright ($f_x = 1.1 \times 10^{-10}$ erg cm^{-2} s^{-1}), hot ($T = 9$ keV) and relatively nearby ($z = 0.051$, Remillard, private communication). Like Ophiuchus (Arnaud *et al.* 1987), its low galactic latitude has resulted in it being overlooked optically. The authors encourage further X-ray and optical studies of this cluster as it lies on the super-galactic plane and close (in redshift) to the Shapley supercluster (Shapley 1930; Scaramella *et al.* 1989 and Raychaudhury 1989).

(ii) Cygnus-A – as reported by Arnaud *et al.* (1987), the *EXOSAT* data show evidence for a non-thermal source at the centre of the cluster containing Cygnus-A. Including an absorbed power law in the fit, a temperature of $5.0^{+4.6}_{-0.9}$ keV, a cluster 2–10 keV luminosity of 6.70×10^{44} erg s^{-1} and iron abundance of $0.40^{+0.38}_{-0.21}$ solar for the cluster are obtained, in agreement with Arnaud *et al.* (1987). Due to the large systematic uncertainty in the temperature, the results for this cluster are not included in our later study. The results obtained are consistent, however, with those found in other clusters.

(iii) A3558 – the *EXOSAT* observation of A3558 was mistakenly positioned on the centre of the *HEAO-1* error box. This resulted in the cluster being offset by 38 arcmin from the centre of the ME field of view. Despite this, a temperature of $3.7^{+2.0}_{-1.0}$ keV and corrected 2–10 keV flux of 4.2×10^{-11} erg cm^{-2} s^{-1} were determined. This cluster is the dominant member of the Shapley supercluster. Although A3558 is not the most X-ray luminous of these clusters (which is A3571), it is one of three clusters that lie in a chain with A3562. As no LE data were available for this observation, due to the large offset, it was not included in this analysis.

(iv) 2059 − 247 – this cluster is the most distant detected by *EXOSAT* ($z = 0.188$). The cluster is reported by White *et al.* (1981) to show a soft spectrum in the *Einstein Observatory* IPC, which they interpret as the evidence that the cluster is at an early stage of evolution. From their analysis of the *EXOSAT* observation, Kaastra & de Korte (1988) quote a temperature of > 5 keV and a luminosity of 2.8×10^{45} erg s^{-1}. So 2059 − 247 is a high-luminosity cluster, but is by no means unusual compared with other nearby clusters. The best-fitting Raymond & Smith temperature is $7.0^{+6.9}_{-2.2}$ keV (assuming an iron abundance of 0.35) with a flux of 7.4×10^{-12} erg cm^{-2} s^{-1}.

(v) A3825/7 – the error box for 1H2159-60 (Piccinotti *et al.* 1982) contains two Abell clusters. The LE image shows both the Abell clusters in the error box are detected. The confusion of these sources in the ME means that little can be said about the spectra of either cluster except that neither are brighter than 1.7×10^{-11} erg cm^{-2} s^{-1}. The LE data were used in the deprojection analysis but the spectra were not analysed.

5 RESULTS

5.1 LE images

The limited sensitivity of the LE made morphological classification of the images difficult. Only A1367 appeared to

have an unusual structure as previously noted by Bechtold *et al.* (1983).

Fig. 2 shows two full sets of deprojection analysis results. Table 3 gives the input parameters for the deprojection analysis of the surface brightness profiles. A summary of the results from the deprojection analysis is given in Table 4. All errors quoted are 3σ except for the mass flow rate where they are the 10 and 90 percentiles.

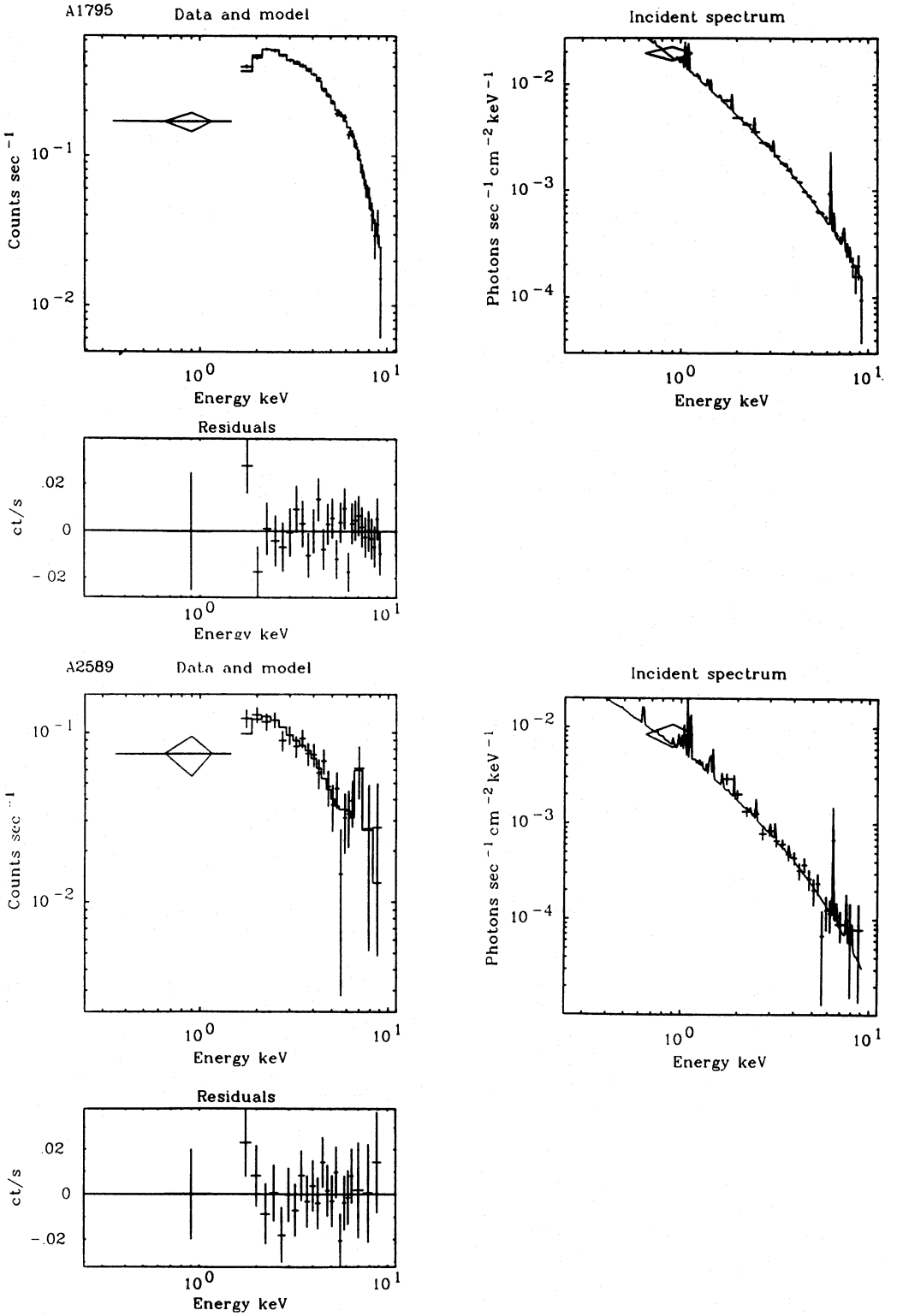

Figure 1. Examples of combined LE and ME spectral fits for A1795 and A2589. The data with the best-fitting model (and residuals below) are plotted on the left and the photon spectra are plotted on the right.

Table 1. Table of *EXOSAT* targets. The clusters marked with asterisks are those that were not observed by the *Einstein Observatory*. The clusters marked with daggers were not included in the correlation analysis. The LE count rates are integrated within 1 Mpc or 20 arcmin, whichever is smallest. The ME count rates are between channels 8 and 38, corresponding to a range of approximately 2–10 keV. The Me count rates in brackets are corrected for the collimator response for clusters offset by more than 10 arcmin from the pointing position.

Cluster	Date	Pointing Position (1950)	X-ray Position (1950)	LE Filter	Exposure (seconds)	LE Count Rate (count s^{-1})	ME Count Rate (count s^{-1} $half^{-1}$)
A22*†	330/83	00 18 12 −25 59 00	–	3LX	7177.3	< 0.01	0.00±0.04
A98†	205/84	00 43 44 +20 14 47	–	3LX	60183.2	< 0.01	0.11±0.04
A119	331/84	00 53 48 −01 34 29	00 53 35.3 −01 30 47	3LX	28014.9	0.09 ± 0.03	2.53±0.04
A133	224/83	01 00 18 −22 04 00	01 00 14.1 −22 09 04	3LX 3LX	L1 17408.8 L2 19575.7	0.07 ± 0.02 0.10 ± 0.02	1.33±0.04
A140*†	327/84	01 02 04 −24 16 50	–	3LX	13361.5	< 0.01	0.10±0.03
A193*	361/84	01 22 25 +08 24 32	01 22 28.0 +08 26 20	3LX	23841.9	0.05 ± 0.02	1.13±0.03
A262	224/84	01 49 51 +35 54 15	01 49 46.7 +35 53 42	3LX	18146.6	0.12 ± 0.03	2.20±0.05
A376	12/85	02 42 32 +36 37 37	02 42 58.3 +36 41 58	3LX	22263.2	0.09 ± 0.02	0.80±0.05
AWM7	258/84	02 51 23 +41 25 26	02 51 11.8 +41 21 39	3LX	16560.3	0.14 ± 0.02	7.79±0.05
A400	13/85	02 54 52 +05 48 22	02 55 03.0 +05 49 32	3LX	38937.2	0.14 ± 0.02	0.73±0.04
A3122*	2/84	03 16 12 −44 16 34	03 16 12.7 −44 24 53	3LX AL/P	4774.5 2364.0	0.05 ± 0.02 0.04 ± 0.02	1.64±0.06
Perseus (A426)	–	Several pointings (See Branduardi-Raymont *et al.* 1985)	03 16 27.7 +41 19 49	3LX 3LX AL/P AL/P BOR BOR	L1 50308.6 L2 8627.0 L1 9295.6 L2 9577.5 L1 9997.9 L2 13321.3	– – – – – –	– – – – – –
0336+096	264/84	03 35 57 +09 48 22	03 35 52.1 +09 48 10	3LX	34983.9	0.18 ± 0.02	4.14±0.05
A478	276/84	04 10 48 +10 22 18	04 10 40.4 +10 20 06	3LX	19357.8	0.03 ± 0.01	5.28±0.04
0422-086*	48/85	04 23 15 −08 40 42	04 23 26.2 −08 40 10	3LX	26442.8	0.04 ± 0.01	1.38±0.06
A496	49/86	04 30 00 −13 16 00	04 31 18.2 −13 21 25	3LX	21670.7	0.06 ± 0.02	2.51±0.04 (4.45±0.07)
3C129	271/85	04 46 14 +45 00 42	04 46 30.0 +44 56 56	3LX	23969.6	0.06 ± 0.02	7.15±0.04
A576	306/84	07 17 24 +55 50 59	07 17 09.1 +55 49 05	3LX	20192.6	0.09 ± 0.03	1.60±0.03
0745-191	304/85	07 45 27 −19 08 30	07 45 18.1 −19 10 14	3LX	40309.9	0.017 ± 0.005	4.46±0.03
A754	323/85	09 05 46 −09 24 44	09 06 55.5 −09 29 22	3LX	23705.5	0.07 ± 0.03	4.76±0.04 (6.60±0.06)
Hydra-A	324/85	09 17 09 −12 04 42	09 15 41.4 −11 53 02	3LX	26113.1	0.07 ± 0.02	1.04±0.04 (1.94±0.07)
A1060	4/84	10 34 30 −27 16 06	10 34 22.3 −27 15 58	3LX	21007.5	0.19 ± 0.02	3.81±0.06
A1318*†	335/84	11 33 58 +55 16 14	–	3LX	14910.2	< 0.01	-0.01±0.05
A1367	5/84	11 41 53 +20 06 59	Highly Diffuse	3LX AL/P	12290.3 16102.5	0.20 ± 0.05 0.07 ± 0.03	2.90±0.06
Virgo	–	Several Pointings (See Edge & Stewart 1988)	12 28 16.9 +12 40 02	3LX 3LX AL/P BOR BOR	L1 36083.8 L2 43684.6 L1 24889.7 L1 12039.9 L2 42702.7	– – – – –	– – – – –
Coma (A1656)	–	Several Pointings (See Hughes *et al.* 1988)	12 57 18.8 +28 13 24	3LX	51171.9	–	–
Centaurus (A3526)	20/84	12 46 00 −41 02 02	12 46 02.8 −41 02 28	3LX	81565.8	0.24 ± 0.03	10.67±0.10
A3558*†	52/86	13 22 15 −31 06 25	Out of FOV	–	–	–	0.69±0.04 (3.40±0.19)
A3562	176/84	13 29 24 −31 25 56	13 30 47.7 −31 24 52	3LX	38987.9	0.08 ± 0.01	2.17±0.06 (3.17±0.09)
A3571*	29/84	13 44 58 −32 35 02	13 44 31.8 −32 38 08	3LX AL/P	8477.5 4226.4	0.21 ± 0.04 0.18 ± 0.03	9.14±0.07
A1795	17/85	13 46 48 +26 51 27	13 46 32.5 +26 50 22	3LX	46466.6	0.17 ± 0.03	4.34±0.03

Table 1 – *continued*

Cluster	Date	Pointing Position (1950)	X-ray Position (1950)	LE Filter	Exposure (seconds)	LE Count Rate (count s^{-1})	ME Count Rate (count s^{-1} $half^{-1}$)
A1837	23/85	13 59 17 −10 54 28	13 58 53.9 −10 54 08	3LX	16651.5	0.02 ± 0.01	0.47±0.05
A2052	68/85	15 14 26 +07 13 44	15 14 16.7 +07 12 12	3LX	32459.4	0.18 ± 0.02	2.43±0.05
A2142	55/86	15 56 12 +27 22 00	15 56 15.7 +27 22 40	3LX	17468.8	0.07 ± 0.01	5.79±0.04
				AL/P	4575.0	0.04 ± 0.02	
A2147	93/84	15 58 56 +16 05 00	15 59 44.1 +16 07 28	3LX	31563.9	0.08 ± 0.03	2.16±0.07 (2.71±0.09)
A2199	208/84	16 26 54 +39 39 43	16 26 54.8 +39 39 41	3LX	4910.8	0.30 ± 0.05	5.93±0.04
				AL/P	6912.2	0.13 ± 0.03	
				BOR	4889.6	0.05 ± 0.02	
Triangulum Australis	197/85	16 31 11 −64 20 24	16 33 36.88 −64 13 50	3LX	36416.0	0.03 ± 0.01	10.47±0.14 (13.91±0.20)
Ophiuchus	250/84	17 09 35 −23 19 58	17 09 25.8 −23 18 28	3LX	17082.7	0.12 ± 0.03	33.64±0.09
A2315†	215/84	19 01 09 +69 52 43	–	3LX	13733.8	< 0.01	0.02±0.05
Cygnus-A†	305/85	19 57 37 +40 33 03	19 57 45.3 +40 35 55	3LX	17876.4	0.035 ± 0.010	5.95±0.05
2059-247†	304/84	20 59 09 −24 45 49	20 59 09.0 −24 45 49	3LX	18819.1	0.006 ± 0.002	0.60±0.04
A3825*†	152/85	21 56 04 −60 19 58	21 55 06.3 −60 34 18	3LX	10889.9	0.012 ± 0.004	1.14±0.07
A3827			21 58 26.3 −60 10 46			0.011 ± 0.004	
S1101 (Sers159-03)	161/84	23 11 16 −42 59 50	23 11 09.7 −43 00 08	3LX	5156.6	0.07 ± 0.02	0.83±0.05
				AL/P	1594.3	0.04 ± 0.02	
A2589*	171/84	23 21 23 +16 32 37	23 21 26.7 +16 29 28	3LX	15781.3	0.08 ± 0.02	1.33±0.07
A4059*	338/84	23 54 26 −35 02 14	23 54 24.8 −35 02 21	3LX	28334.8	0.12 ± 0.02	1.66±0.04
	200/84	23 55 23 −35 01 40			(combined)		

Table 2. List of previously published results from *EXOSAT* data on clusters.

Cluster	Paper	Temperature (keV)	Iron Abundance (solar)	Mass Flow Rate ($M_\odot\ yr^{-1}$)
0336+096	1,2	2.9±0.3	0.4±0.2	14–200
		(3.1±0.3)	($0.35^{+0.25}_{-0.23}$)	(105–180)
0745-191	3	$8.6^{+1.1}_{-0.9}$	$0.33^{+0.11}_{-0.11}$	440–930
		($8.5^{+1.8}_{-1.4}$)	($0.29^{+0.14}_{-0.16}$)	(430–1020)
A1060	4	3.2	–	3–14
		($3.3^{+0.4}_{-0.3}$)	(<0.46)	(2–19)
Cygnus-A	3	$4.1^{+5.6}_{-1.5}$	$0.59^{+0.68}_{-0.35}$	–
		($5.0^{+4.6}_{-1.4}$)	($0.40^{+0.38}_{-0.21}$)	(51–113)
Ophiuchus	3	$9.4^{+1.5}_{-1.2}$	$0.26^{+0.14}_{-0.13}$	150–220
		($9.0^{+0.8}_{-0.7}$)	($0.28^{+0.07}_{-0.07}$)	(17–160)
2008-569	4	$5.3^{+1.1}_{-0.9}$	$0.57^{+0.20}_{-0.27}$	–
		(-)	(-)	(-)
2059-247	5	>6.0	–	800
		($7.0^{+6.9}_{-2.2}$)	(0.35 fixed)	(120–440)

Notes: [1]Singh, Westergaard & Schnopper (1986); [2]Singh, Westergaard & Schnopper (1988b); [3]Arnaud *et al.* (1987); [4]Singh, Westergaard & Schnopper (1988a); [5]Piro & Fusco-Femiano (1988); [6]Kaastra & de Korte (1988).

5.2 Spectra

The results from the spectral fits using the emission code of Raymond & Smith (1977) are given with the 90 per cent confidence errors in Table 5. The results are quoted in the cluster rest frame. Of the 45 clusters presented here, five were too faint to give a reliable spectrum. The results are consistent with previous spectral measurements. Fig. 3 shows the comparison of *EXOSAT* with *HEAO-1* A-2 temperatures (Mushotzky 1984) and reveals a systematic difference between the measurements at low temperature. The iron abundance determinations from *HEAO-1* (Rothenflug & Arnaud 1985) are also consistent with those presented here apart from 0336 + 096 which is anomalously high in *HEAO-1* (1.2 compared to 0.35 with *EXOSAT*). A comparison of *EXOSAT* ME and *Einstein Observatory* MPC temperatures is presented in Edge *et al.* (1990).

From the spectral results in Table 5, and assuming values for H_0 of 50 km s^{-1} Mpc^{-1}, h of 1 and q_0 of 0.5, 2–10 keV luminosities can be calculated. After correction for galactic absorption and bandwidth, bolometric luminosities were also determined (see Paper II).

The additional X-ray data used (Table 6) comes from the *Einstein Observatory* from the deprojection results of Arnaud (1988) and King profile fitting by Abramopoulos & Ku (1983) (AK) and Jones & Forman (1984) (JF). The methods of profile fitting used by the two groups were different (see Section 6.3) so both datasets are treated separately.

5.3 Iron lines

The most prominent spectral feature of clusters between 2 and 10 keV is the iron line complex at 6.7 keV from the $K\sigma$ transition. The ME spectra were fitted with thermal bremsstrahlung models with and without an iron line to determine the significance of the feature. For 27 of the 40 cluster spectra, the F-test (e.g. Bevington 1969) shows that a line is required at a significance level greater than 90 per cent.

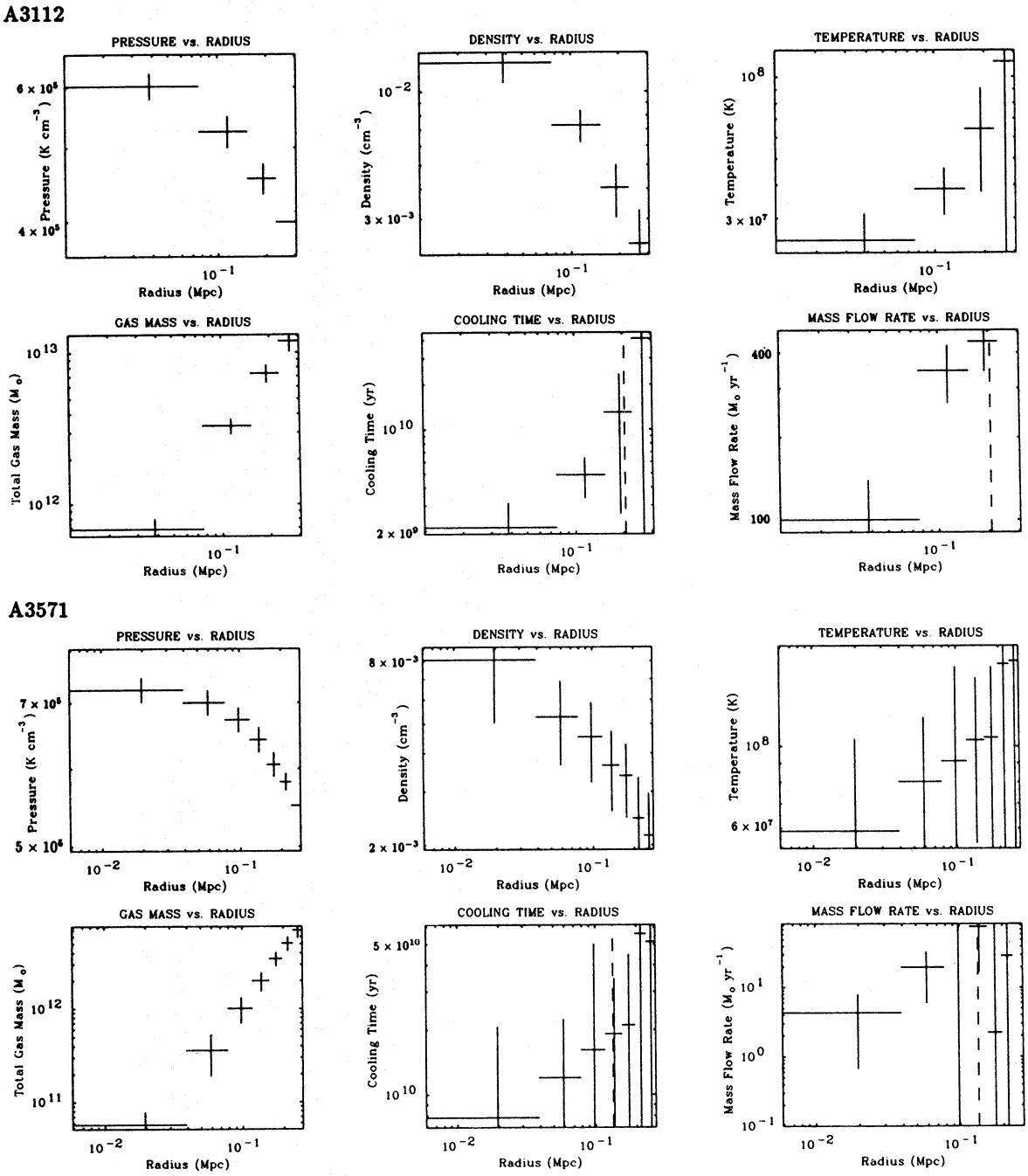

Figure 2. Examples of LE deprojection analysis for A3112 and A3571. The dashed vertical line marks the average cooling radius. The plotted errors are 90 per cent confidence.

Several spectra also required the addition of a second $K\beta$ line at 7.9 keV. The ratios of $K\alpha$ to $K\beta$ line strengths have large uncertainties but are consistent with the values expected for plasmas in ionization equilibrium at the appropriate temperature.

The values obtained for the iron abundance using the emission code of Raymond & Smith (1977) are shown plotted against the cluster luminosity in Fig. 4. The mean iron abundance is 0.32 with an rms deviation of 0.18. Only one cluster (Coma) has an abundance significantly different from the mean (0.21 ± 0.03). These results are in general agreement with *GINGA* results (Hatsukade 1989; Butcher & Stewart 1990) and those of Rothenflug & Arnaud (1985) from *HEAO-1*, but the mean abundance is lower than the value of 0.42 they obtained (after correction for the different Fe/H ratio of 3.2×10^{-5} assumed by these authors).

5.4 Column densities

The hydrogen column densities derived from the spectral fits are compared with those expected from 21-cm line emission (Heiles 1975; Stark *et al.*, private communication) in Fig. 5. The results show good agreement and in only two cases was the galactic value above the 90 per cent confidence upper limit (A400 and 0745 – 191). A derived column density which is too low could indicate a low-energy excess (e.g. a

Table 3. Input parameters for deprojection analysis.

Cluster	Redshift	Number Of Bins	Bin Size (arcsec)	Outer Radius (kpc)	Velocity Dispersion (kms s^{-1})	Core Radius (Mpc)	Overall Temperature (keV)	Outer Pressure (10^4 K cm^{-3})
A119	0.044	3	124	379.3	778	0.5	5.1	10
A133	0.0604	9	23	322.8	700	0.4	4.0	20
A193	0.0482	4	108	504.5	700	0.4	4.0	6
A262	0.0164	5	21	44.3	415	0.4	2.4	10
A376	0.0489	3	56	189.4	800	0.4	5.1	30
AWM7	0.017	5	40	88.5	830	0.4	3.5	20
A400	0.0232	6	145	525.7	423	0.5	2.2	4
A3112	0.0746	4	38	267.1	820	0.4	4.0	40
Perseus	0.0184	17	36	321.3	1100	0.2	5.5	45
0336+09	0.0349	5	40	176.4	700	0.4	3.1	38
A478	0.0882	7	30	455.3	1100	0.2	6.8	22
0422-08	0.039	4	105	400.7	600	0.4	3.0	7
A496	0.032	6	54	364.9	657	0.4	4.7	22
3C129	0.022	4	93	203.7	750	0.4	5.6	10
A576	0.0381	4	90	335.8	914	0.5	3.8	10
0745-19	0.1028	5	26	333.1	1200	0.4	8.5	120
A754	0.0528	6	36	288.1	1048	0.4	8.9	35
Hydra-A	0.0522	9	36	440.4	800	0.4	3.9	18
A1060	0.0114	7	46	98.2	676	0.2	3.3	13
Virgo	(15 Mpc)	24	36	63.7	500	0.2	2.5	50
Coma	0.0232	14	72	664.5	800	0.4	6.8	10
Centaurus	0.0109	14	32	135.5	586	0.4	3.6	32
A3562	0.0478	6	18	134.5	800	0.4	3.8	40
A3571	0.039	7	36	255.1	900	0.4	7.7	55
A1795	0.0616	11	30	529.7	821	0.3	5.0	22
A1837	0.0376	5	72	379.0	500	0.4	2.4	6
A2052	0.0348	8	40	293.1	576.	0.3	3.6	25
A2142	0.0899	6	45	589.2	1241	0.4	11.0	40
A2147	0.0365	3	96	245.5	1132	0.4	4.4	20
A2199	0.0309	11	34	311.0	807	0.2	4.7	20
Tri. Aust.	0.051	5	108	638.9	900	0.4	8.0	10
Ophiuchus	0.028	9	36	384.8	1000	0.4	9.0	20
Cygnus-A	0.057	5	72	562.9	800	0.2	4.2	12
2059-24	0.188	5	36	801.3	1000	0.4	9.0	30
A3825	0.0744	4	72	576.9	800	0.4	5.0	5
A3827	0.0993	4	72	749.6	800	0.4	7.0	7
S1101	0.0544	5	25	171.3	550	0.4	2.8	35
A2589	0.0421	5	32	168.9	602	0.4	3.6	28
A4059	0.0478	13	28	203.9	700	0.4	3.5	30

cooling flow). 0745−191 has a very large cooling flow (M=400–1000 $M_\odot$ yr^{-1}) suggesting that this is indeed the source of the discrepancy. The relatively large errors on the integrated LE count rates prevented a significant detection of a low-energy excess in any of the other large cooling flow clusters in this sample from combined LE and ME fits.

6 CORRELATIONS BETWEEN X-RAY PROPERTIES

The data presented in this paper provide the largest spectral dataset currently available. From the 45 observations, five clusters were too faint and four were excluded due to

Table 4. Results from deprojection analysis. The clusters marked with asterisks had outer pressures normalized to the pressure profile from deprojection of IPC data.

Cluster	Redshift	Central Density (10^{-3} cm^{-3})	Central Temperature (10^7 K)	Central Cooling Time (10^9 yr)	Cooling Radius (kpc)	Mass Flow Rate 10,50 and 90 % Percentiles ($M_\odot$ yr^{-1})	Gas Mass in 200kpc (10^{12} $M_\odot$)
A119	0.044	2.3±0.5	3.3±1.2	15.±9.	91±38	0 , 23 , 38	3.6±1.5
A133	0.0604	10.4±2.8	2.0±1.0	2.6±2.8	175±58	98 , 128 , 163	3.6±0.3
A193	0.0482	1.6±0.5	5.1±3.1	32±38	–	0 , 0 , 17	2.6±0.9
A262*	0.0164	12.2±3.8	0.7±0.4	0.9±1.4	34±2	8 , 16 , 29	–
A376	0.0489	5.3±1.4	3.7±1.4	7.2±4.8	95±36	9 , 26 , 48	–
AWM7*	0.017	8.9±2.6	1.7±0.9	2.8±3.7	66±9	8 , 25 , 42	–
A400*	0.0232	1.8±0.6	2.2±1.4	19±25	81±67	0 , 8 , 32	2.5±1.0
A3112	0.0746	13.1±2.3	2.5±0.6	2.1±1.0	205±95	334 , 430 , 565	7.9±0.9
Perseus	0.0184	42.0±2.6	3.2±0.2	0.73±0.07	192±8	338 , 393 , 417	6.6±0.2
0336+09	0.0349	17.8±1.0	1.4±0.1	0.9±0.1	131±14	105 , 142 , 181	–
A478	0.0882	17.8±2.0	5.3±0.9	2.3±0.6	257±86	212 , 571 , 992	8.3±1.1
0422-08	0.039	4.3±0.3	1.3±0.1	3.4±0.6	124±47	41 , 56 , 83	3.7±1.4
A496*	0.032	9.8±1.5	1.8±0.4	2.2±0.9	177±52	74 , 121 , 215	4.1±0.6
3C129	0.022	7.8±2.2	3.6±1.7	5.1±4.5	124±32	28 , 61 , 95	4.5±1.4
A576	0.0381	2.6±0.9	4.2±2.4	18±19	38±40	0 , 25 , 98	3.5±1.0
0745-19	0.1028	19.8±2.7	5.2±0.8	2.1±0.5	228±38	430 , 702 , 1020	12±2
A754	0.528	6.1±2.2	5.5±3.8	10±13	94±48	3 , 24 , 52	3.4±0.7
Hydra-A	0.0522	12.6±1.9	2.0±0.4	1.8±0.7	224±63	234 , 316 , 489	5.6±0.6
A1060*	0.0114	8.8±2.2	1.3±0.8	2.2±3.3	67±22	2 , 9 , 19	–
Virgo	(15 Mpc)	165±4	0.47±0.02	0.03±0.01	49±1	6 , 10 , 13	–
Coma	0.0232	2.7±0.6	5.6±2.0	17±12	43±23	0 , 2 , 5	2.3±0.1
Centaurus	0.0109	22.1±1.7	1.0±0.1	0.5±0.1	79±20	10 , 18 , 25	–
A3562	0.0478	9.5±3.7	3.2±1.9	4.5±4.8	100±25	12 , 45 , 65	–
A3571	0.039	8.1±3.1	5.9±4.6	8±13	134±63	7 , 71 , 150	4.4±0.7
A1795*	0.0616	16.8±0.9	2.3±0.3	1.5±0.1	266±16	470 , 512 , 556	6.8±0.1
A1837	0.0376	3.1±0.8	1.7±0.9	7.7±9.4	131±77	5 , 18 , 93	6.1±1.3
A2052	0.0348	12.3±0.7	1.2±0.8	1.1±0.2	149±26	68 , 90 , 114	3.0±0.4
A2142	0.0899	8.5±1.1	7.4±1.2	5.8±1.3	204±31	180 , 244 , 312	8.4±0.8
A2147	0.0365	3.6±1.0	6.1±3.8	15±25	126±63	0 , 54 , 88	4.3±0.6
A2199*	0.0309	14.1±3.5	2.9±1.2	2.4±1.8	181±33	103 , 150 , 204	4.0±0.4
Tri. Aust.	0.051	13.6±4.5	8.9±12.3	65±254	–	0 , 0 , 0	2.4±1.3
Ophiuchus	0.028	15.7±4.2	4.4±3.6	3.1±7.4	130±52	17 , 75 , 159	5.0±0.6
Cygnus-A	0.057	6.1±0.7	2.1±0.4	3.9±1.0	129±56	51 , 73 , 113	5.4±0.8
2059-24	0.188	6.3±1.2	6.4±3.2	8.0±8.9	204±61	122 , 242 , 442	9.9±2.4
A3825	0.0744	1.3±0.5	4.8±3.2	41±56	–	0 , 0 , 10	2.4±1.3
A3837	0.0993	1.1±0.4	8.3±6.1	67±96	–	0 , 0 , 0	3.5±1.6
S1101	0.0544	16.2±4.0	1.5±0.7	1.3±1.5	133±14	159 , 251 , 365	–
A2589	0.0421	8.3±2.5	2.3±1.3	3.9±4.0	115±22	15 , 46 , 80	–
A4059	0.0478	10.0±2.8	2.4±2.0	3.5±8.5	155±28	80 , 124 , 173	–

confusion or high redshift, leaving 36 clusters. The X-ray parameters are plotted against each other in Figs 6–10. The best-fitting least-squared lines and correlation coefficients are given in Table 7. All X-ray properties were also tested for a correlation with redshift which might introduce an indirect correlation between other parameters (Table 7). All the correlations between X-ray properties are, in fact, direct.

6.1 Luminosity and temperature

The two principal X-ray parameters are the X-ray luminosity and temperature of the cluster. These are plotted in Fig. 6 and show a strong correlation as previously noted by Smith *et al.* (1979), Mitchell *et al.* (1979) and Mushotzky (1988). There is a significant scatter at all temperatures which is

Table 5. Table of spectral results from RS fits. All errors are 90 per cent confidence. The quoted fluxes are corrected for collimator response for pointings offset by more than 10 arcmin from the source and large extent (i.e. Virgo, Coma, Perseus and Ophiuchus).

Cluster	Temperature (keV)	Iron Abundance (relative to solar)	Column Density ($\times 10^{21}$ cm^{-2})	Galactic Column ($\times 10^{21}$ cm^{-2})	2-10 keV Flux ($\times 10^{-11}$ ergs cm^{-2} s^{-1})	χ^2 for fit
A119	$5.1^{+1.0}_{-0.8}$	$0.28^{+0.26}_{-0.25}$	$0.23^{+1.33}_{-0.14}$	0.36	3.02	27.04 (25)
A133	$3.8^{+2.0}_{-0.9}$	< 1.1	$0.28^{+0.99}_{-0.26}$	0.40	1.43	24.60 (17)
A193	$4.2^{+1.6}_{-0.9}$	$0.57^{+0.64}_{-0.54}$	$0.30^{+3.78}_{-0.28}$	0.42	1.34	20.74 (22)
A262	$2.4^{+0.3}_{-0.3}$	$1.3^{+0.9}_{-0.7}$	$0.16^{+0.89}_{-0.05}$	0.49	2.34	12.73 (22)
A376	$5.1^{+3.2}_{-1.9}$	< 0.70	$0.24^{+0.94}_{-0.09}$	0.58	1.01	17.51 (20)
AWM7	$3.6^{+0.2}_{-0.2}$	$0.43^{+0.28}_{-0.25}$	$0.59^{+0.45}_{-0.09}$	0.88	9.08	53.50 (25)
A400	$2.1^{+1.3}_{-0.5}$	< 4.6	< 0.75	0.85	0.79	21.07 (22)
A3112	$4.1^{+2.3}_{-1.1}$	$0.81^{+0.96}_{-0.71}$	$0.28^{+1.93}_{-0.16}$	0.40	1.94	23.70 (19)
0336+09	$3.1^{+0.3}_{-0.3}$	$0.35^{+0.25}_{-0.23}$	$0.61^{+1.10}_{-0.19}$	1.40	4.65	23.37 (27)
A478	$6.8^{+1.1}_{-1.0}$	$0.27^{+0.14}_{-0.16}$	$1.1^{+1.9}_{-0.7}$	1.30	6.54	32.39 (30)
0422-09	$2.9^{+0.9}_{-0.6}$	< 1.6	$0.34^{+0.95}_{-0.11}$	0.60	1.60	19.22 (18)
A496	$4.7^{+1.0}_{-0.8}$	< 0.51	$0.6^{+2.1}_{-0.1}$	0.45	5.37	20.44 (25)
3C129	$5.6^{+0.7}_{-0.6}$	$0.20^{+0.11}_{-0.11}$	$6.2^{+2.3}_{-1.9}$	5.76	9.00	39.23 (33)
A576	$3.7^{+0.8}_{-0.6}$	$0.43^{+0.48}_{-0.41}$	< 8.8	0.62	1.72	17.57 (22)
0745-19	$8.5^{+1.9}_{-1.4}$	$0.29^{+0.14}_{-0.16}$	$2.9^{+2.0}_{-1.4}$	4.61	5.71	32.08 (29)
A754	$8.7^{+1.8}_{-1.6}$	< 0.37	$0.48^{+1.89}_{-0.11}$	0.42	8.48	38.47 (30)
Hydra-A	$3.9^{+1.0}_{-0.9}$	< 0.41	< 6.1	0.47	2.44	27.24 (23)
A1060	$3.3^{+0.4}_{-0.3}$	< 0.46	$0.21^{+0.61}_{-0.05}$	0.50	4.35	17.04 (26)
A1367	$3.5^{+0.5}_{-0.5}$	< 0.29	$0.20^{+0.33}_{-0.13}$	0.20	3.44	20.39 (22)
Centaurus	$3.6^{+0.4}_{-0.4}$	$0.47^{+0.28}_{-0.26}$	$0.28^{+1.24}_{-0.08}$	0.80	11.22	31.81 (29)
A3562	$3.8^{+1.0}_{-0.8}$	< 1.2	$0.29^{+0.28}_{-0.13}$	0.45	3.62	16.63 (20)
A3571	$7.6^{+1.2}_{-0.9}$	$0.38^{+0.17}_{-0.18}$	$0.24^{+0.50}_{-0.05}$	0.42	12.26	27.16 (25)
A1795	$5.1^{+0.4}_{-0.5}$	$0.25^{+0.14}_{-0.12}$	$0.11^{+0.10}_{-0.03}$	0.11	5.30	28.98 (25)
A1837	$2.4^{+0.9}_{-0.8}$	< 11.	< 5.8	0.48	0.50	27.01 (22)
A2052	$3.4^{+0.6}_{-0.5}$	$0.53^{+0.52}_{-0.43}$	$0.30^{+0.89}_{-0.13}$	0.27	2.62	28.78 (19)
A2142	$11.0^{+2.0}_{-1.7}$	< 0.36	$0.33^{+0.99}_{-0.13}$	0.38	7.48	29.34 (36)
A2147	$4.4^{+2.2}_{-1.1}$	< 1.1	$0.53^{+1.86}_{-0.19}$	0.35	3.27	25.67 (23)
A2199	$4.7^{+0.4}_{-0.4}$	$0.21^{+0.13}_{-0.13}$	$0.07^{+0.06}_{-0.03}$	0.09	7.12	30.74 (28)
Tri. Aust.	$8.0^{+1.4}_{-1.3}$	$0.24^{+0.18}_{-0.16}$	$2.5^{+1.8}_{-1.0}$	2.00	11.03	34.82 (34)
Ophiuchus	$9.0^{+0.8}_{-0.7}$	$0.29^{+0.07}_{-0.08}$	$2.0^{+0.9}_{-0.7}$	1.97	43.63	36.75 (27)
S1101	$3.0^{+1.2}_{-0.7}$	< 1.5	$0.04^{+0.25}_{-0.04}$	0.20	0.95	16.54 (19)
A2589	$3.7^{+2.2}_{-1.1}$	< 2.1	$0.15^{+2.22}_{-0.09}$	0.46	1.61	13.02 (19)
A4059	$3.5^{+0.6}_{-0.6}$	< 0.92	$0.16^{+0.23}_{-0.08}$	0.11	1.88	19.84 (27)

much larger than the measurement errors. This scatter can be understood if one notes that the X-ray luminosity is dependent on the density and temperature in the form:

$$L_{\rm bol} \propto \int_{\rm vol} \rho^2 T^{1/2}\, dV. \qquad (1)$$

For gas distributions with the same shape, a variation in the central density from cluster to cluster would introduce some dispersion in the X-ray luminosity. Fig. 11 illustrates this density variation by splitting the sample into clusters with central densities above and below 9×10^{-3} cm^{-3}. A clear difference between the samples is seen, with the denser clusters a factor of three brighter than the others.

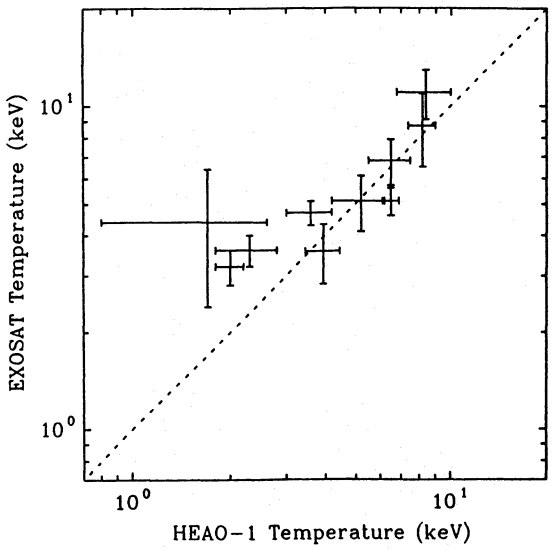

Figure 3. *EXOSAT* temperatures against *HEAO-1* temperatures.

Table 6. Additional X-ray data from the literature. The core radii for Centaurus and Hydra-A are from Matilsky, Jones & Forman (1985) and David *et al.* (1990) respectively, but are determined using the same technique as Jones & Forman (1984). The gas masses are from deprojection analysis of the *Einstein Observatory* data by Arnaud (1988).

Cluster	Redshift	Core Radius from Abramopoulos & Ku (Mpc)	Core Radius from Jones & Forman (Mpc)	Gas Mass within 0.5 Mpc (10^{12} M$_\odot$)
A119	0.0440	0.77±0.06	–	10.7±0.7
A133	0.0604	0.26±0.02	–	12.9±0.6
A262	0.0161	–	0.10±0.03	–
A376	0.0489	–	–	9.3±1.4
A400	0.0232	0.35±0.05	0.17±0.03	4.8±0.4
Perseus	0.0184	–	0.29±0.05	–
A478	0.0882	–	–	34.5±1.6
A496	0.032	0.22±0.02	–	12.4±0.5
3C129	0.022	–	–	5.5± 0.4
A576	0.0381	0.39±0.05	0.12±0.03	9.0±0.7
A754	0.0528	0.71±0.05	–	–
Hydra-A	0.0522	–	0.15±0.04	–
A1060	0.0114	–	0.10±0.01	–
A1367	0.0215	–	0.48±0.12	–
Centaurus	0.0109	–	0.09±0.02	–
Coma	0.0232	0.50±0.02	0.31±0.03	16.0±0.4
A1795	0.0616	–	0.30±0.10	22.9±0.7
A2052	0.0348	0.22±0.02	–	11.2±0.7
A2142	0.0899	0.51±0.02	–	30.2±1.2
A2199	0.0309	–	0.14±0.02	–
S1101	0.0556	–	–	12.1±1.5

On the assumption that the gas is isothermal within 0.5 Mpc then the total gravitational mass within that radius is $3.9\times10^{13}\,(T/\mathrm{keV})\,M_\odot$ (from hydrostatic equilibrium). From the correlation between gas mass and X-ray luminosity, the gas mass within 0.5 Mpc can be calculated as $5.5\times10^{-6}\,(L_{\mathrm{bol}}^{0.41}/\mathrm{erg\ s^{-1}})\,M_\odot$. Thus the ratio of the gas mass to total mass within the core of the sample clusters can be determined. This ratio is plotted in Fig. 12 and shows a scatter of a factor of three (~4 to 12 $h^{-3/2}$ per cent).

The 'shape' of the cluster density profile could also influence the total X-ray luminosity. Two clusters with identical masses of gas would have different luminosities if one had a highly peaked density profile and the other had a broad one. This would introduce a large scatter in the relationship of core gas mass and X-ray luminosity which is not evident in Fig. 7.

Incomplete thermalization of the ICM gas due to turbulence (Loewenstein & Fabian 1990), which would affect the measured gas temperature differently from cluster to cluster, could also cause scatter in the temperature–luminosity correlation. This is consistent with the X-ray data, but may imply much larger scatter between temperature and optical parameters, such as galaxy density and velocity dispersion, than is seen (Paper II).

The present data cannot be used to differentiate conclusively between all the possibilities, although the variation of the ICM mass fraction is the most plausible. Future imaging spectral data will be able to measure unambiguously both the total mass and gas mass, allowing any possible mass fraction variation to be quantified.

6.2 Cooling flows

The majority of clusters (~ 90 per cent) in this sample are cooling to some extent in their cores. This is consistent with the proportion seen in the flux-limited sample (Stewart, Edge & Fabian, in preparation), but is higher than found previously using the *Einstein Observatory* (Stewart *et al.* 1984; Arnaud 1988). The lower fraction of cooling flows seen by the *Einstein Observatory* may result from the spatial resolu-

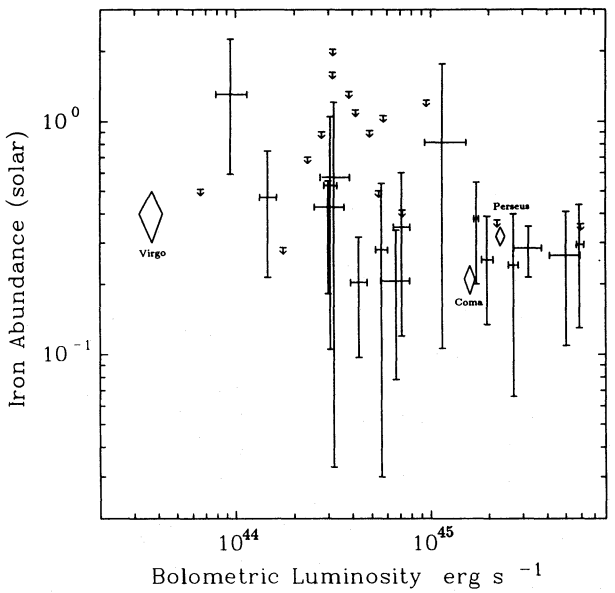

Figure 4. Iron abundance against bolometric X-ray luminosity.

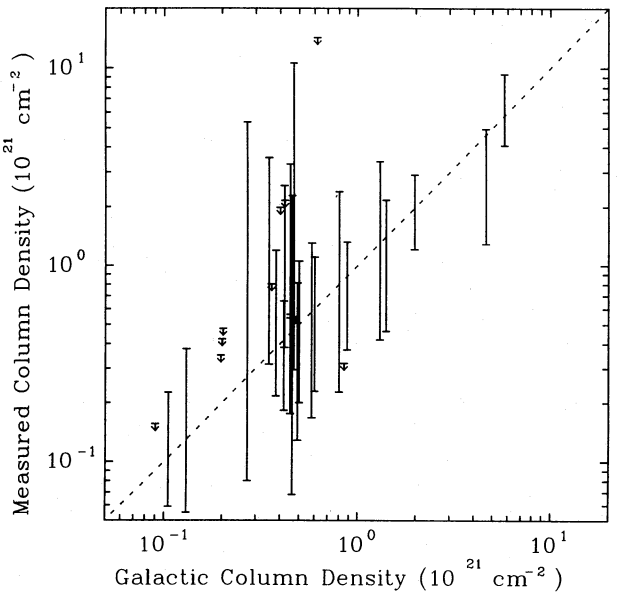

Figure 5. Measured column density against predicted column density from 21-cm measurements from Stark *et al.* (private communication). The dashed line represents equal galactic and measured columns.

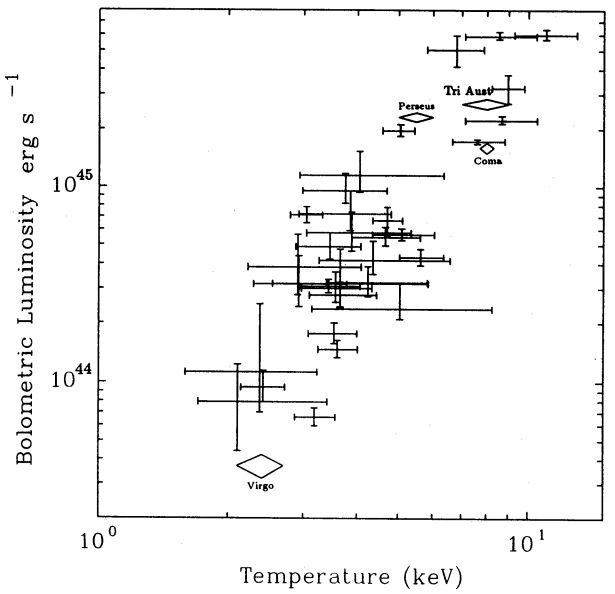

Figure 6. Bolometric X-ray luminosity against temperature. Four of the brightest clusters (Virgo, Coma, Perseus & Triangulum Australis) are marked with diamonds.

tion of the IPC and the larger fraction of high-redshift clusters in the previous samples. The implication of this result is that cooling flows are common and therefore long-lived. Hence the integrated mass deposited in the central 100–200 kpc can reach 10^{12-13} $M_{\odot}$ in a Hubble time, i.e. the mass of a massive, central galaxy. Although the inferred star formation rate from optical observations is only a few per cent of the mass flow rate (Johnstone, Fabian & Nulsen 1987), the resulting mass-to-light ratio for the central galaxy agrees with other values (~ 30–100, i.e. a few per cent of the deposited mass).

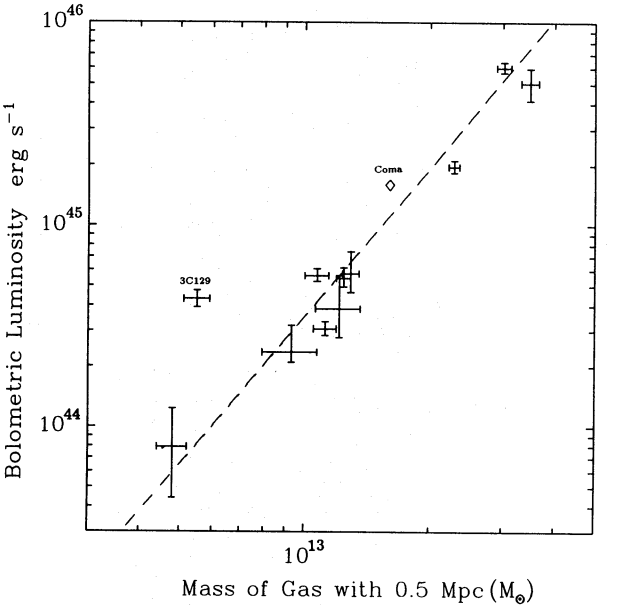

Figure 7. Bolometric X-ray luminosity against gas mass within 0.5 Mpc determined from deprojection analysis.

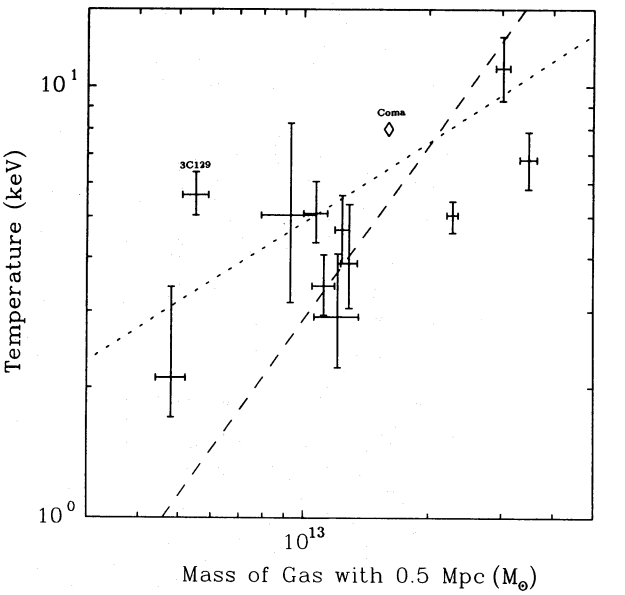

Figure 8. Temperature against gas mass within 0.5 Mpc.

6.3 Core radius

The correlations of the X-ray properties with core radius show a general trend but with a large scatter (Figs 9 and 10), as seen by Hatsukade (1989). The correlations are plotted to show the difference between the core radii from AK and JF as they are determined using different assumptions. In the case of AK, they assume a value of β from the temperature and velocity dispersion or if those data are not available assume β = 1 and fit the profile using that value, whereas JF allow β to be a free variable. Also JF exclude the central bins where there is a cooling flow. There appears to be a systematic difference between the two determinations of a factor of

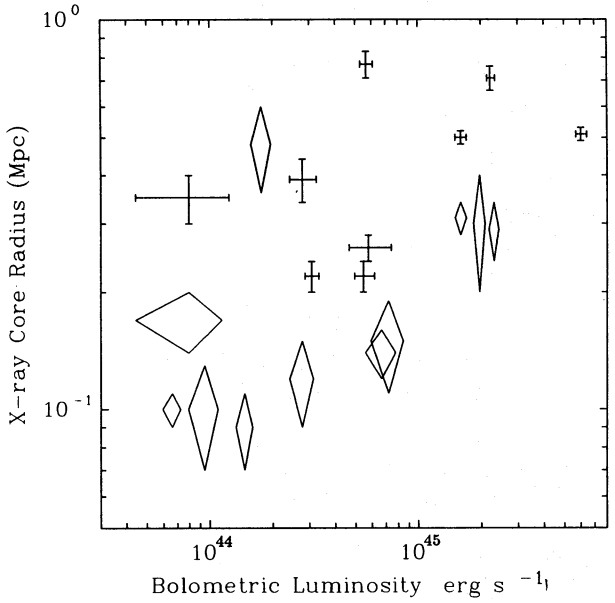

Figure 9. Bolometric X-ray luminosity against core radius. Diamonds are data from Jones & Forman (1984) and crosses from Abramopoulos & Ku (1983).

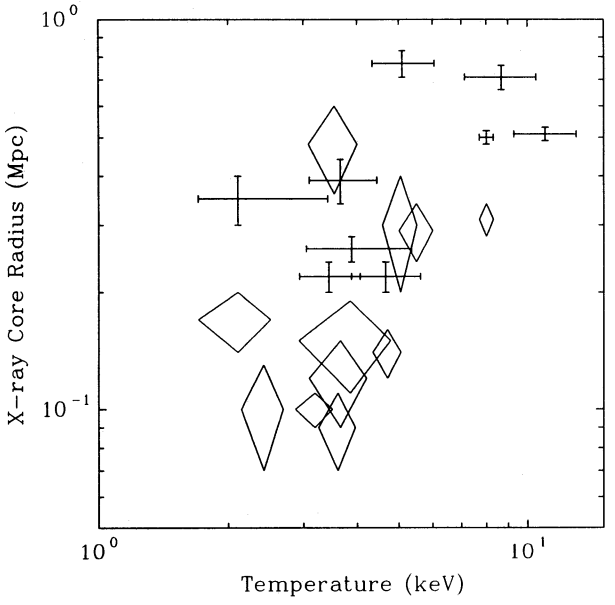

Figure 10. Temperature against core radius. The symbols are as in Fig. 9.

Table 7. Table of correlation results for X-ray data. The results are from least-squares fits of the form $Y = 10^B \times X^A$ and the errors are 90 per cent significance. The X-ray luminosities are in erg s^{-1}, the temperatures in keV and the gas masses in solar masses.

	L_{2-10}	L_{Bol}	T	z	$M_{0.5Mpc}$
		L_{2-10} vs. L_{Bol}	L_{2-10} vs. T	L_{2-10} vs. z	L_{2-10} vs. $M_{0.5Mpc}$
L_{2-10}		A=1.07±0.02 B=-3.51±0.08 r=0.998 n=36	A=2.79±0.05 B=42.54±0.03 r=0.900 n=36	A=1.85±0.04 B=47.21±0.05 r=0.826 n=36	A=2.59±0.07 B=10.50±0.09 r=0.981 n=12
	L_{Bol} vs. L_{2-10}		L_{Bol} vs. T	L_{Bol} vs. z	L_{Bol} vs. $M_{0.5Mpc}$
L_{Bol}	A=0.94±0.03 B=3.02±0.15 r=0.998 n=36		A=2.62±0.10 B=43.05±0.08 r=0.864 n=36	A=1.39±0.06 B=47.06±0.08 r=0.748 n=36	A=2.45±0.16 B=12.69±0.18 r=0.967 n=12
	T vs. L_{2-10}	T vs. L_{Bol}		T vs. z	T vs. $M_{0.5Mpc}$
T	A=0.28±0.05 B=-11.73±0.20 r=0.870 n=36	A=0.30±0.05 B=-12.73±0.23 r=0.850 n=36		A=0.22±0.10 B=1.06±0.15 r=0.302 n=36	A=0.62±0.24 B=-7.37±0.28 r=0.607 n=12
	z vs. L_{2-10}	z vs. L_{Bol}	z vs. T		z vs. $M_{0.5Mpc}$
z	A=0.29±0.01 B=-14.23±0.01 r=0.820 n=36	A=0.32±0.01 B=-15.68±0.02 r=0.831 n=36	A=0.71±0.01 B=-1.79±0.01 r=0.642 n=36		A=0.62±0.03 B=-9.42±0.03 r=0.589 n=12
	$M_{0.5Mpc}$ vs. L_{2-10}	$M_{0.5Mpc}$ vs. L_{Bol}	$M_{0.5Mpc}$ vs. T	$M_{0.5Mpc}$ vs. z	
$M_{0.5Mpc}$	A=0.38±0.03 B=-3.77±0.17 r=0.957 n=12	A=0.41±0.05 B=-5.26±0.19 r=0.960 n=12	A=0.74±0.10 B=12.66±0.09 r=0.667 n=12	A=0.55±0.08 B=13.98±0.11 r=0.653 n=12	

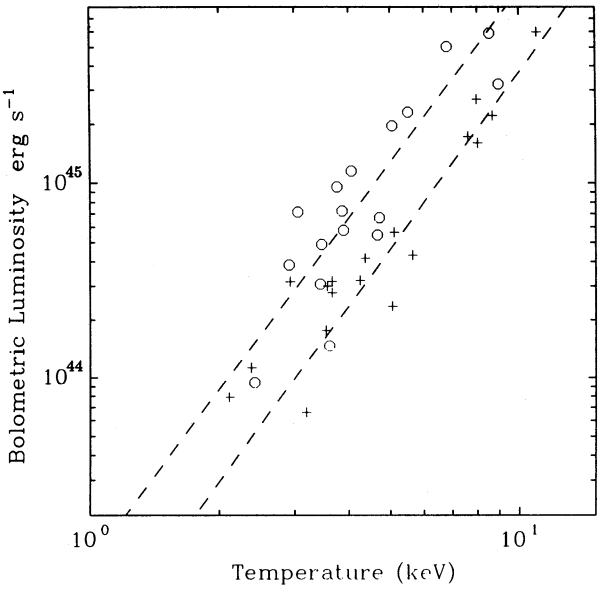

Figure 11. X-ray luminosity against temperature split on density. The crosses are for clusters with central densities less than 9×10^{-3} cm^{-3} and the circles above 9×10^{-3} cm^{-3}. The dashed lines are the best-fitting lines for the two subsamples.

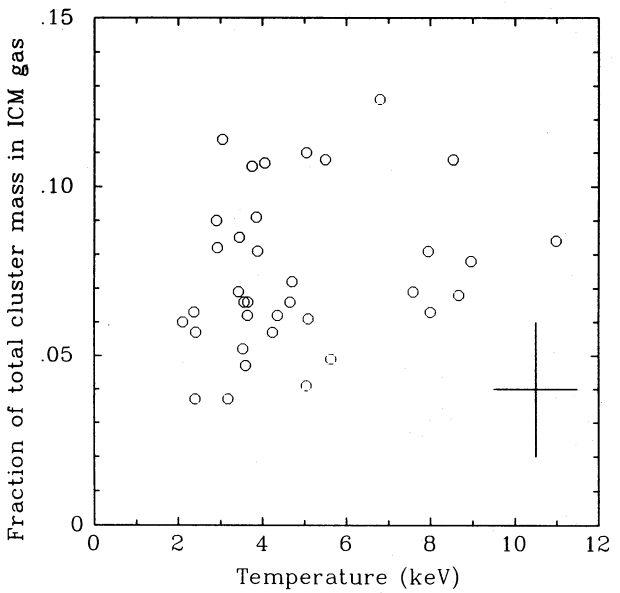

Figure 12. Inferred ratio of gas mass to total mass within 0.5 Mpc plotted against temperature. A sample error bar is marked.

~2, although a substantial scatter remains. This scatter may be due largely to the difficulty in determining core radii from surface brightness profiles, but may also reflect the evolutionary state of the cluster. For instance, A1367 has a highly irregular X-ray structure (Bechtold *et al.* 1983) and large core radius but a moderately low temperature, therefore lying off the core radius-temperature correlation. So 'unrelaxed' clusters have not developed the 'core' seen in other dynamically older clusters. Due to the uncertainties in the core radii, no correlation results are quoted although the trend is for $T \propto r_{\rm core}$.

The general trend for hotter, more luminous clusters to be 'larger' could affect the luminosity–temperature correlation. However, as the gas mass within 0.5 Mpc is also a function of the core radius, the scatter in the gas mass-luminosity relation should reflect the importance of the core radius. The scatter seen in Fig. 7 is at most a factor of two, hence setting an upper limit to any scatter introduced by core radius variations. This is much less than the factor of 10 seen in Fig. 6. Therefore the conclusion that the variation of gas mass, rather than the distribution of the gas, is the dominant source of scatter is unaffected.

7 CONCLUSIONS

The sample of 45 clusters observed with *EXOSAT* presented here provide a number of new insights into the X-ray properties of clusters. The imaging data provided by *EXOSAT* indicate that the large majority of the clusters in the sample are cooling at some level. This implies that cooling flows are the norm in clusters, not the exception. The high frequency of cooling flows has important consequences for the development of cD galaxies in clusters.

The high-quality spectral data indicate that the ratio of the gas mass to total mass in the central 0.5 Mpc varies by a factor of three between the clusters in the sample. The derived iron abundances show no significant trend with temperature or luminosity. These two observations have important implications for models of the ICM. First, the variable gas–mass ratio implies that the gas production rate within each cluster has been different from cluster to cluster. Secondly, as the abundance of iron in clusters is relatively constant, the gas is produced at a single abundance (~0.3 solar) for all clusters. The implications of these results and the prospects for future X-ray work are discussed in more detail in Paper II.

ACKNOWLEDGMENTS

The authors thank the *EXOSAT* Observatory staff for the smooth operation of the satellite and the database during and after the mission, and Andy Fabian, Ofer Lahav and Jackie Butcher for comments on the paper and encouragement during the analysis. Richard Mushotzky is particularly thanked for his valuable comments and criticism. ACE and GCS acknowledge the support of the SERC through a studentship and Advanced Fellowship. ACE also acknowledges the support of the Royal Society during the completion of this paper.

REFERENCES

Abramopoulos, F. & Ku, W., 1983. *Astrophys. J.*, **271**, 446.
Arnaud, K. A., 1988. In: *Cooling Flows in Galaxies and Clusters*, p. 31, ed. Fabian, A. C., Kluwer Academic Publishers, Dordrecht.
Arnaud, K. A., Johnstone, R. M., Fabian, A. C., Crawford, C. S., Nulsen, P. E. J., Shafer, R. A. & Mushotzky, R. F., 1987. *Mon. Not. R. astr. Soc.*, **227**, 241.
Bechtold, J., Forman, W., Giacconi, R., Jones, C., Schwartz, J., Tucker, W. & Van Speybroeck, L., 1983. *Astrophys. J.*, **265**, 26.
Bevington, P. R., 1969. *Data Reduction and Error Analysis for the Physical Sciences*, McGraw-Hill Book Company, New York.
Branduardi-Raymont, G., Kellett, B., Fabian, A. C., McGlynn, T., Manzo, G. & Peacock, A., 1985. *Adv. Space Res.*, **5**, 3, 133.

Butcher, J. A. & Stewart, G. C., 1990. Preprint, University of Leicester.
Cavaliere, A. & Fusco-Femiano, R., 1976. *Astr. Astrophys.*, **49**, 137.
David, L. P., Arnaud, K. A., Forman, W. & Jones, C., 1990. *Astrophys. J.*, **356**, 32.
de Korte, P. A. J., Bleeker, J. A. M., den Boggende, A. J. F., Branduardi-Raymont, G., Brinkman, A. C., Culhane, J. L., Gronenschild, E. H. B. M., Mason, I. & McKechnie, S. P., 1981. *Space Sci. Rev.*, **30**, 495.
de Young, D. S., 1978. *Astrophys. J.*, **223**, 47.
Edge, A. C., 1989. *Ph D thesis*, University of Leicester.
Edge, A. C. & Stewart, G. C., 1988. In: *Proc. Hot Thin Plasmas in Astrophysics, NATO ASI*, p. 335, ed. Pallavicini, R., Reidel, Dordrecht.
Edge, A. C. & Stewart, G. C., 1991. *Mon. Not. R. astr. Soc.*, **252**, 428 (Paper II).
Edge, A. C., Stewart, G. C., Fabian, A. C. & Arnaud, K. A., 1990. *Mon. Not. R. astr. Soc.*, **245**, 559.
Fabian, A. C., Hu, E. M., Cowie, L. L. & Grindlay, J., 1981. *Astrophys. J.*, **248**, 47.
Hatsukade, 1989. *PhD thesis*, University of Osaka.
Heiles, C., 1975. *Astr. Astrophys. Suppl.*, **20**, 37.
Hughes, J. P., Gorenstein, P. & Fabricant, D., 1988. *Astrophys. J.*, **329**, 82.
Johnstone, R. M., Fabian, A. C. & Nulsen, P. E. J., 1987. *Mon. Not. R. astr. Soc.*, **224**, 75.
Jones, C. & Forman, W., 1978. *Astrophys. J.*, **224**, 1.
Jones, C. & Forman, W., 1984. *Astrophys. J.*, **276**, 38.
Kaastra, J. S. & de Korte, P. A. J., 1988. *Astr. Astrophys.*, **192**, 77.
Kowalski, M. P., Ulmer, M. P., Cruddace, R. G. & Wood, K. S., 1984. *Astrophys. J. Suppl.*, **56**, 403.
Loewenstein, M. & Fabian, A. C., 1990. *Mon. Not. R. astr. Soc.*, **242**, 120.
McHardy, I. M., Lawrence, A., Pye, J. P. & Pounds, K. A., 1981. *Mon. Not. R. astr. Soc.*, **197**, 893.
Matilsky, T., Jones, C. & Forman, W., 1985. *Astrophys. J.*, **291**, 621.
Mitchell, R. J., Dickens, R. J., Bell Burnell, S. J. & Culhane, J. L., 1979. *Mon. Not. R. astr. Soc.*, **189**, 329.
Mushotzky, R. F., 1984. *Phys. Scr.*, Vol. **T7**, 157.
Mushotzky, R. F., 1988. In: *Hot Thin Plasmas in Astrophysics, Proc. NATO ASI*, p. 273, ed. Pallavicini, R., Reidel, Dordrecht.
Mushotzky, R. F., Serlemitsos, P. J., Smith, B. W., Boldt, E. A. & Holt, S. S., 1978. *Astrophys. J.*, **225**, 21.
Peacock, A., Andreson, R. D., Manzo, G., Taylor, B. G., Villa, G., Re, S., Ives, J. C. & Kellock, S., 1981. *Space Sci. Rev.*, **30**, 525.
Piccinotti, G., Mushotzky, R. F., Boldt, E. A., Holt, S. S., Marshall, F. E., Serlemitsos, P. J. & Shafer, R. A., 1982. *Astrophys. J.*, **253**, 485.
Piro, L. & Fusco-Femiano, R., 1988. *Astr. Astrophys.*, **205**, 26.
Raychaudhury, S., 1989. *Nature*, **342**, 251.
Raymond, J. C. & Smith, B. W., 1977. *Astrophys. J. Suppl.*, **35**, 419.
Rothenflug, R. & Arnaud, M., 1985. *Astr. Astrophys.*, **144**, 431.
Sarazin, C. L., 1988. *X-ray Emissions from Clusters of Galaxies*, Cambridge University Press, Cambridge.
Scaramella, R., Baiesi-Pillastrini, G., Chincarini, G., Vettolani, G. & Zamorani, G., 1989. *Nature*, **338**, 562.
Shapley, H., 1930. *Bull. Harvard Obs.*, **874**, 9.
Singh, K. P., Westergaard, N. J. & Schnopper, H. W., 1986. *Astrophys. J.*, **308**, L51.
Singh, K. P., Westergaard, N. J. & Schnopper, H. W., 1988a. *Astrophys. J.*, **330**, 620.
Singh, K. P., Westergaard, N. J. & Schnopper, H. W., 1988b. *Astrophys. J.*, **331**, 672.
Smith, B. W., Mushotzky, R. F. & Serlemitsos, P., 1979. *Astrophys. J.*, **227**, 37.
Stewart, G. C., Fabian, A. C., Jones, C. & Forman, W., 1984. *Astrophys. J.*, **285**, 1.
Turner, M. J. L., Smith, A. & Zimmerman, H. U., 1981. *Space Sci. Rev.*, **30**, 479.
White, N. E. & Peacock, A., 1988. *Mem. Soc. Astr. Ital.*, **59**, 1–2, 7.
White, R. A., Sarazin, C. L., Quintana, H. & Jaffe, W. J. 1981. *Astrophys. J. Lett.*, **245**, L1.